J. Fluid Mech. (1994), *vol.* 267, *pp.* 251–273

On the stability of vertical double-diffusive interfaces. Part 2. Two parallel interfaces

By I. A. ELTAYEB[1] AND D. E. LOPER[2]

[1] Department of Mathematics and Computing, Sultan Qaboos University, Muscat, Sultanate of Oman

[2] Department of Mathematics, Florida State University, Tallahassee, FL 32306, USA

(Received 20 July 1993 and in revised form 23 November 1993)

This is the second part of a three-part study of the stability of vertically oriented double-diffusive interfaces having an imposed vertical stable temperature gradient. In this study, flow is forced within a fluid of infinite extent by a prescribed excess of compositionally buoyant material between two parallel interfaces. Compositional diffusivity is ignored while thermal diffusivity and viscosity are finite. The stability of the interfaces is analysed first in the limit that they are close together (compared with the salt-finger lengthscale), then for general spacing. Attention is focused on whether the preferred mode of instability is varicose or sinuous and whether its wavevector is vertical or oblique.

The interfaces are found to be unstable for some wavenumber for all values of the Prandtl number and interface spacing. The preferred mode of instability for closely spaced interfaces is varicose and vertical for Prandtl number less than about 9, sinuous oblique for Prandtl number between 9 and 15 and sinuous vertical for larger Prandtl number. For general spacing each of the four possible modes of instability is preferred for some range of Prandtl number and interface separation, with no clear pattern of preference, except that the sinuous oblique mode is preferred for widely separated interfaces. The growth rate of the preferred mode is largest for interfaces having separations of from 1 to 3 salt-finger lengths.

1. Introduction

This is the second of a three-part study of the stability of vertically oriented double-diffusive interfaces. The first part (Eltayeb & Loper 1990; herein referred to as Part 1) considered the stability of a single plane interface. In the present study we consider the stability of two plane parallel interfaces. This analysis is a stepping stone toward the physically most interesting case of a circular cylindrical interface, to be studied in the third part.

Specifically we consider a vertical slab of compositionally buoyant fluid sandwiched between two semi-infinite regions containing fluid which is compositionally less buoyant, although the analysis is valid for the opposite arrangement. This configuration is sometimes referred to as a Cartesian plume. Material diffusivity is assumed to be negligibly small so that the interfaces remain sharp and well defined. The conditions under which this assumption is valid are discussed in §5.4 of Part 1. A stabilizing vertical thermal gradient is imposed on the system.

In the absence of diffusion a static stable solution exists in which the slab of compositionally buoyant fluid has a uniform temperature deficit such that no density contrast exists across the interfaces. If the fluids on either side of the interfaces are

allowed to interact via exchange of heat and momentum, a static state is no longer possible. Thermal diffusion alters the density of the fluid close to the interfaces and this density difference induces a steady vertical motion. This flow and the associated thermal field are referred to as the *basic state*. The basic-state solution for the parallel interfaces being studied here has been presented in §3.2 of Part 1 (see equations (1:3.10) and (1:3.11)),† and graphed in figure 1:3. We shall investigate the stability of this basic-state flow to instabilities in the form of harmonic distortions of the plane interfaces.

It was found in Part 1 that for an arbitrarily small compositional difference, the basic-state solution for the single plane interface is unstable for some range of wavenumbers for all values of the Prandtl number, σ. For most values σ, the preferred mode of instability is oblique; that is, the interface has variations in both the horizontal and vertical directions. This is in marked contrast to studies of flow next to a heated vertical wall (Gill 1966; Gill & Davey 1969; Dudis & Davis 1971; Holyer 1983) which found only vertical modes (i.e. modes having no variation in the horizontal direction) to be most unstable.

A related problem, investigated by Lister (1987), concerns the stability of a slab of dense fluid of thickness $2a$ falling down the centre of a plane channel of width $2A$ otherwise filled with a less-dense fluid. Lister found that in the limit $a/A \to 0$, the plume is unstable to vertical long-wavelength perturbations. The present study differs from that of Lister in three respects. First, no thermal effects are included in his analysis while temperature variations, both in the vertical and the horizontal, play an important role in our analysis. This difference makes the two analyses fundamentally distinct. Secondly, the dense fluid is allowed to have a different viscosity from the surrounding fluid in Lister's analysis, whereas we restrict attention to fluids having identical viscosities. This limitation eliminates from our problem the possible occurrence of instabilities driven by viscosity contrast (Schneider 1981; Hinch 1984). Third, the basic flow in Lister's problem fills the channel and in the limit $a/A \to 0$ takes an arbitrarily long time to establish from an initial state of rest, whereas in our problem the basic flow decays exponentially with distance from the interface, and thus can be established in a relatively short time.

In what follows we shall investigate the effect on the stability of the single plane interface of the addition of a second interface a distance $2X_0$ from it, forming a Cartesian plume. The instability is manifest as a distortion of the two interfaces. The modes of instability may be characterized by the symmetry of the distortions, with a *varicose* mode having deflections of the interfaces out of phase, and a *sinuous* mode having deflections in phase. Also of interest is the question of whether the preferred mode of instability is *vertical* or *oblique*. We shall see that each of the four types of instability is preferred for some range of plume thickness and Prandtl number.

This paper is organized as follows. The stability mechanism of the single interface is discussed in §2, with emphasis on the reason why an oblique instability is preferred. The results of Part 1 discussed in §2 form one limiting case of the present analysis: an extremely wide Cartesian plume ($X_0 \to \infty$). In order to gain better insight into the behaviour of the Cartesian plume, the opposite limiting case of a thin plume ($X_0 \to 0$) is considered in §4, following the formulation of the full problem in §3. It is not obvious whether the thin plume will be unstable, neutral or stable in the limit $X_0 \to 0$; this question is addressed in §4. The full problem of a general plume (of arbitrary thickness) is analysed in §5. The results of the analyses are summarized in §6.

† In what follows equation $(x.y)$ of Part 1 will be referred to as $(1:y.x)$, and figure z of Part 1 will be referred to a figure $1:z$.

In the interest of brevity, the algebraic details of the analysis are not presented here. These details are summarized in three appendices which are available upon request from the editorial office of this Journal or from either author. Appendix A contains the solution details for the thin plume, Appendix B contains those for the plume of arbitrary width and it is shown in Appendix C that the general solution presented in Appendix B reduces to that of Appendix A in the limit of a thin plume.

2. Discussion of the instability of the single plane interface

In Part 1 it was found that a sharp compositional interface across which momentum and heat may diffuse is prone to an oblique instability which occurs for any non-zero value of the compositional difference. The timescale, τ, for growth of the instability is

$$\tau = \left[\frac{\nu\rho}{(\Delta\rho)_c}\right]^2 \frac{\alpha\gamma}{\kappa g}, \tag{2.1}$$

where ρ is the density, $(\Delta\rho)_c$ is the compositional density contrast across the interface, ν is the kinematic viscosity, α is the coefficient of thermal expansion, κ is the thermal diffusivity, g is the acceleration due to gravity and γ is the imposed stable temperature gradient.

The influence of thermal diffusion is to enhance instability, while viscosity is stabilizing for nearly all wavelengths. At the simplest level of analysis, this effect is apparent in (2.1); an increase of κ increases the growth rate of the instability, while an increase of ν decreases this rate.

The interface is unstable to perturbations of all finite wavelengths if the Prandtl number is less than 1.472. For larger values of the Prandtl number the interface becomes stable for moderate vertical wavelengths and large horizontal wavelengths; however, the interface is unstable to perturbations of some wavelength for all values of Prandtl number. The preferred mode of instability is vertical if the Prandtl number is less than 0.065, while for larger values, oblique disturbances are preferred. The (dimensionless) wavelengths of the preferred modes are of unit order, indicating that the instability occurs on the salt-finger lengthscale, $(\nu\kappa/\alpha\gamma g)^{\frac{1}{4}}$.

A striking feature of the results of Part 1 is that for all but very small values of the Prandtl number, oblique instabilities are preferred, in apparent defiance of Squire's theorem (Drazin & Reid 1981). From a cursory analysis of equations (1:4.23)–(1:4.25) (reproduced as (2.7)–(2.9) below) governing w_1, p_1 and T_1, it would appear that vertical instabilities (i.e. those with $m = 0$) would be preferred as m appears explicitly only in the parameter a^2, the increase of which causes a decrease in the strength of the response to the forcing terms. However, the action of m on the zeroth-order variables which appear in the forcing terms on the right-hand sides of these equations is such as to cause an oblique instability to be preferred. It may be seen from figure 1:12 that obliqueness, as measured by the size of the horizontal wavenumber, m, increases in strength with increasing Prandtl number, suggesting that the cause of obliqueness arises principally from the variation with m of the forcing terms on the right-hand side of (1:4.25) (reproduced as (2.9) below). The nature of the instability and the reason for its obliqueness will now be discussed.

The fluid on the positive-x side of the interface (x being the Cartesian coordinate normal to the undisturbed interface) is compositionally dense, while that on the other side is compositionally buoyant. In order that the fluid far from the interface have the same density at the same height, the fluid at x large and positive must be hotter than that at x large and negative. This requires that the basic temperature profile $\bar{T}(x)$ have

a positive gradient in the vicinity of the interface. This gradient, when coupled with the imposed vertical static gradient, makes the unperturbed temperature profile weakly oblique in the vertical plane normal to the undisturbed interface. That is, the gradient of the second of (1:2.12) combined with (1:3.6) evaluated at $x = 0$ yields

$$\nabla T = \frac{\hat{z}}{\sigma R} + \frac{\hat{x}}{2\sqrt{2}},$$

where $\hat{z}$ is the upward unit vector, $\hat{x}$ is a unit vector normal to the undisturbed interface, σ is the Prandtl number and R is a measure of the compositional jump (see (1:2.11) or (3.2)). With $R \ll 1$, the gradient is nearly vertical, but its obliqueness increases with increasing Prandtl number σ. This suggests that the obliqueness of the unperturbed temperature profile in the (x, z)-plane is the cause of the obliqueness of the preferred mode in the (x, y)-plane.

Turning now to a more detailed analysis, we begin by noting that in real notation the harmonic displacement of the interface, given by (1:4.1) (or by (3.9)) with $\Omega = R^2\Omega_2$, is

$$\eta = \epsilon\tilde{\eta} = 2\epsilon \exp(R^2\Omega_2 t)\cos(\zeta), \tag{2.2}$$

where ϵ is a small parameter, t is the dimensionless time and $\zeta = my + nz$. Here y and z are Cartesian coordinates in the plane of the undisturbed interface with z being vertical, and m and n are the horizontal and vertical wavenumbers of the disturbance (each assumed positive). The dimensional form of the timescale R^2t is given by (2.1). The perturbation grows if $\mathrm{Re}[\Omega_2] > 0$, and it follows from the condition $\mathrm{i}u_1(0) = \Omega_2$ that this occurs provided $\mathrm{Re}[\mathrm{i}u_1] > 0$ at the interface. This may be clearly seen by substitution of the small-R expansion (1:4.17) into (1:4.2) (i.e. (3.19) into (3.10)). Noting that the zeroth-order variables are real and the first-order variables are imaginary as employed in Part 1 and making use of (2.2), we obtain to order R

$$\boldsymbol{u}^\dagger \cdot \hat{\boldsymbol{x}} \approx u_0^\dagger + Ru_1^\dagger = u_0 \,\mathrm{d}\tilde{\eta}/\mathrm{d}z + R(\mathrm{i}u_1)\,\tilde{\eta}, \tag{2.3a}$$

$$\boldsymbol{u}^\dagger \cdot \hat{\boldsymbol{z}} \approx w_0^\dagger + Rw_1^\dagger = w_0\,\tilde{\eta} - R(\mathrm{i}w_1)\,\mathrm{d}\tilde{\eta}/\mathrm{d}z, \tag{2.3b}$$

$$p^\dagger \approx p_0^\dagger + Rp_1^\dagger = np_0\,\mathrm{d}\tilde{\eta}/\mathrm{d}z + nR(\mathrm{i}p_1)\,\tilde{\eta}, \tag{2.3c}$$

and

$$T^\dagger \approx T_0^\dagger + RT_1^\dagger = T_0\,\tilde{\eta} - R(\mathrm{i}T_1)\,\mathrm{d}\tilde{\eta}/\mathrm{d}z. \tag{2.3d}$$

Note that $u_1^\dagger$ is in phase with the interface, which is directly displaced if $(\mathrm{i}u_1) > 0$. Recall that u_0, w_1, p_1 and T_1 are odd functions of x while u_1, w_0, p_0 and T_0 are even.

It may be verified by direct calculation of the solutions of the zeroth-order variables, given by (1:4.18), that in the vicinity of the interface with $x > 0$ the signs of the zeroth-order variables are as follows: $u_0 < 0$, $p_0 < 0$ and $T_0 < 0$, with $w_0 > 0$ for small $x (< \sim 1.0)$ and $0 < w_0$ for larger x. The relation between the zeroth-order variables and the deflected interface is depicted in figure 1, together with the behaviour of the basic-state vertical velocity and temperature, $\bar{w}$ and $\bar{T}$. Note that the zeroth-order flow is that necessary to mould the basic-state flow $\bar{w}$ to the distorted interface. Further direct calculation reveals that u_0 and p_0 become more positive (i.e. decrease in magnitude) as m increases (with x held fixed), w_0 becomes more positive and T_0 becomes more negative (increases in magnitude). As we shall see, the decrease in the magnitude of u_0 is the key to triggering an oblique instability.

The character of $(\mathrm{i}u_1)$ may be determined most directly by substitution of expansion (1:4.17) (i.e. (3.19)) into the normal momentum equation (1:4.4). At order R this is

$$(\mathrm{d}^2/\mathrm{d}x^2 - a^2)(\mathrm{i}u_1) = n[\mathrm{d}(\mathrm{i}p_1)/\mathrm{d}x - \bar{w}u_0], \tag{2.4}$$

where

$$a^2 = m^2 + n^2 \tag{2.5}$$

is the square of the wavenumber in the (y, z)-plane. Note that $\Omega_1 = 0$ has been used to

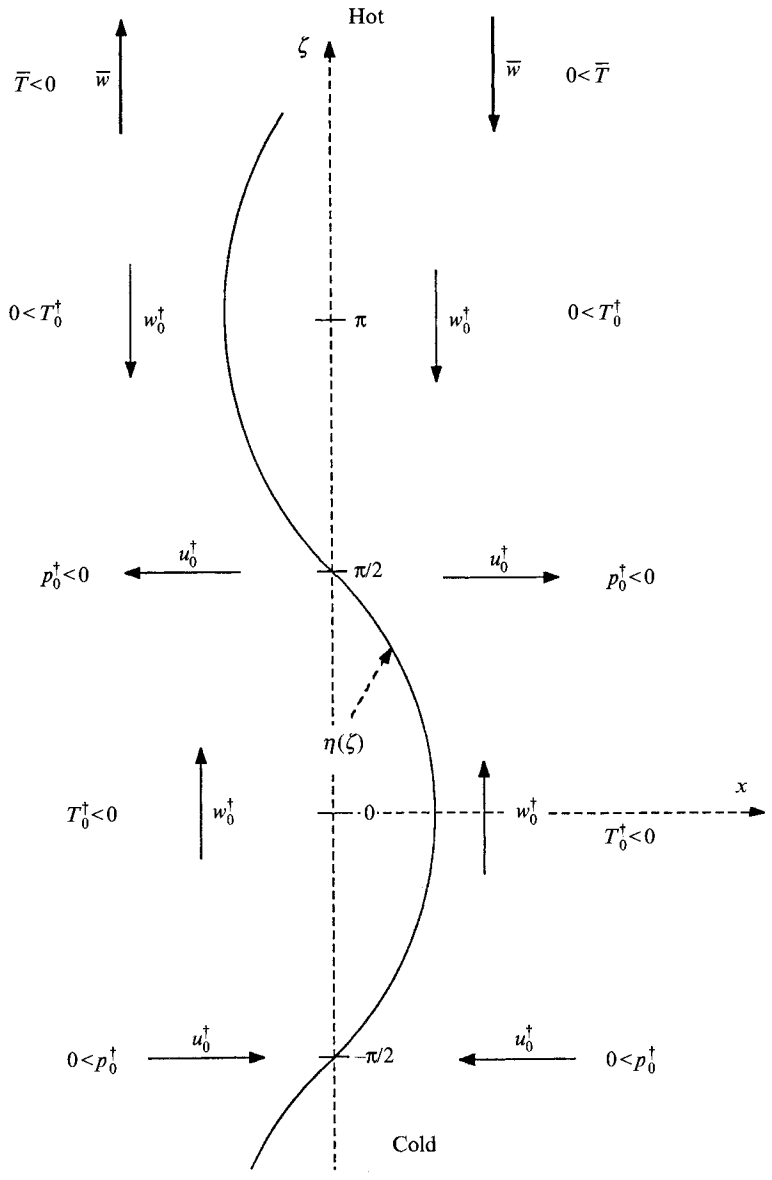

FIGURE 1. A schematic depiction of the basic-state variables and the zeroth-order perturbations in the vicinity of the deformed single plane interface. The solid curved line denotes the deformed interface $x = \eta(\zeta)$ where $\zeta = my + nz$. A static vertical temperature gradient is imposed on the system, making it hot above and cold below. The basic-state velocity $\bar{w}$ is odd in x, being principally downward on the right-hand side of the interface and upward on the left. The basic-state temperature $\bar{T}$ is also odd in x, having a positive gradient in the vicinity of the interface. The presence of this gradient is necessary for the oblique mode of instability to be preferred. The zeroth-order velocity perturbations $u_0^\dagger$ and $w_0^\dagger$ are just those required to mould $\bar{w}$ to the deformed interface.

obtain (2.4). This is a Poisson equation for an even function $(\mathrm{i}u_1)$ having homogeneous boundary conditions. Noting that $\mathrm{d}u_1/\mathrm{d}x(0) = p_1(0) = 0$, we may multiply (2.4) by $\exp(-ax)$ and integrate from 0 to ∞. After some integration by parts, we obtain

$$\Omega_2 = \mathrm{i}u_1(0) = \int_0^\infty \left[\frac{n}{a}\bar{w}(x)\,u_0(x) - nip_1(x)\right]\exp(-ax)\,\mathrm{d}x. \tag{2.6}$$

The first-order variables p_1, w_1 and T_1 are solutions of equations (1:4.23)–(1:4.25) subject to continuity conditions (1:4.28) and suitable decay conditions. Noting the symmetries and complex character of the variables, this problem may be restated in terms of real variables on $0 \leqslant x < \infty$ as follows:

for $0 < x < \infty$

$$(\mathrm{d}^2/\mathrm{d}x^2 - a^2)(\mathrm{i}p_1) = (\mathrm{i}T_1) + 2(\mathrm{d}\bar{w}/\mathrm{d}x)\,u_0, \tag{2.7}$$

$$(\mathrm{d}^2/\mathrm{d}x^2 - a^2)(\mathrm{i}w_1) = -(\mathrm{i}T_1) - n^2(\mathrm{i}p_1) - n\bar{w}w_0 - (\mathrm{d}\bar{w}/\mathrm{d}x)\,u_0, \tag{2.8}$$

$$(\mathrm{d}^2/\mathrm{d}x^2 - a^2)(\mathrm{i}T_1) = (\mathrm{i}w_1) - n\sigma\bar{w}T_0 - \sigma(\mathrm{d}\bar{T}/\mathrm{d}x)\,u_0; \tag{2.9}$$

at $x = 0$:

$$\mathrm{i}p_1 = \mathrm{i}w_1 = \mathrm{i}T_1 = 0. \tag{2.10}$$

Also, the variables decay to zero as $x \to \infty$. Continuity of the derivatives at $x = 0$ is assured by the symmetry of the functions.

Multiplication of (2.7) by $x\exp(-ax)$, integration from 0 to ∞ and integration by parts yields

$$\int_0^\infty \mathrm{i}p_1(x)\exp(-ax)\,\mathrm{d}x = \int_0^\infty \left[-\mathrm{i}T_1(x) - 2\frac{\mathrm{d}\bar{w}}{\mathrm{d}x}(x)\,u_0(x)\right]\left(\frac{x}{2a}\right)\exp(-ax)\,\mathrm{d}x. \tag{2.11}$$

Similarly, multiplication of (2.9) by $(ax^2 + x)\exp(-ax)$, integration from 0 to ∞ and integration by parts yields

$$\int_0^\infty \mathrm{i}T_1(x)\,x\exp(-ax)\,\mathrm{d}x$$

$$= \int_0^\infty \left[-\mathrm{i}w_1(x) + n\sigma\bar{w}(x)\,T_0(x) + \sigma\frac{\mathrm{d}\bar{T}}{\mathrm{d}x}(x)\,u_0(x)\right]\left(\frac{ax^2+x}{4a^2}\right)\exp(-ax)\,\mathrm{d}x. \tag{2.12}$$

Combining (2.6), (2.11) and (2.12) we have

$$\Omega_2 = U_1 + U_2 + U_3, \tag{2.13}$$

where

$$U_j = \int_0^\infty V_j(x)\exp(-ax)\,\mathrm{d}x, \tag{2.14}$$

$$\left.\begin{aligned} V_1(x) &= \frac{n}{a}u_0(x)\frac{\mathrm{d}}{\mathrm{d}x}[x\bar{w}(x)], \quad V_2(x) = -\frac{n}{8a^3}(ax^2+x)\,\mathrm{i}w_1(x), \\ V_3(x) &= \frac{n\sigma}{8a^3}(ax^2+x)\left[n\bar{w}(x)\,T_0(x) + \frac{\mathrm{d}\bar{T}}{\mathrm{d}x}(x)\,u_0(x)\right]. \end{aligned}\right\} \tag{2.15}$$

Using (1:3.5), (1:3.6), (1:B 10), (1:B 11) and (1:B 17), we have

$$U_1 = -\frac{n^2}{2a}\mathrm{Im}\left[\sum_{j=1}^{3}\frac{(\lambda_j + a)\,\lambda_j A_j}{(\lambda_j + k + a)^2}\right], \tag{2.16}$$

$$U_2 = \frac{n}{8a^3}\sum_{j=1}^{3}\frac{(\lambda_j + 3a)}{(\lambda_j + a)^3}\mu_j^3 B_j + \frac{n^2}{16a^3}\mathrm{Im}\left[\sum_{j=1}^{3}\frac{(\lambda_j + k + 3a)}{(\lambda_j + k + a)^3}A_j w_j\right], \tag{2.17}$$

and

$$U_3 = \frac{n^2}{16a^3}\mathrm{Im}\left[\sum_{j=1}^{3}\frac{(\lambda_j + k + 3a)}{(\lambda_j + k + a)^3}A_j(\mu_j^2 - \mathrm{i}k\lambda_j)\right], \tag{2.18}$$

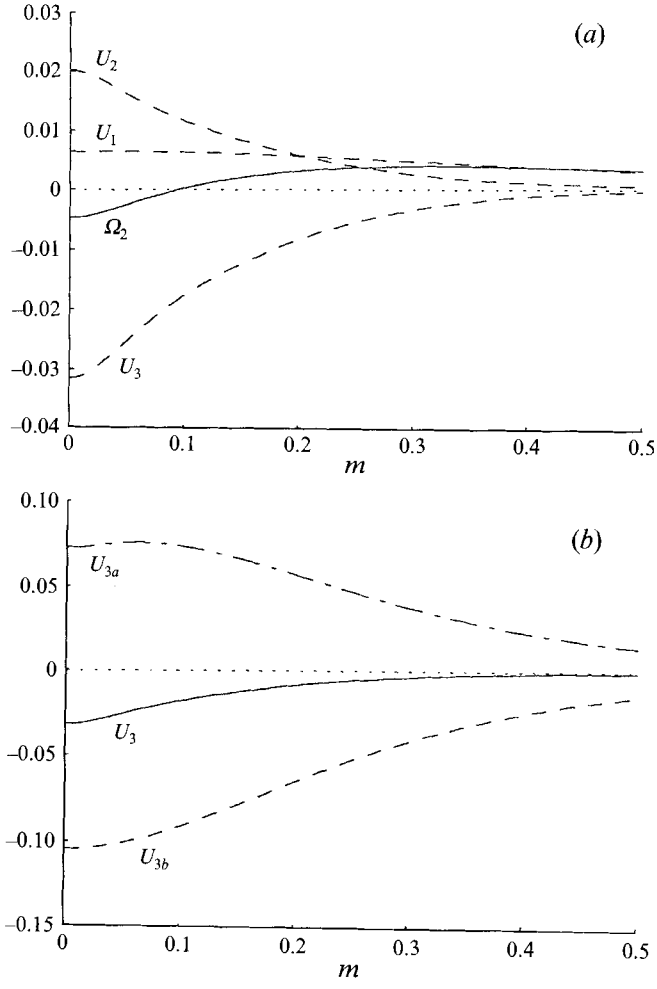

FIGURE 2. Graphs of Ω_2 and its components as a function of m for $\sigma = 5.0$ and $n = 0.38$. The magnitude of σ was chosen to be close to that of water, then the value of n taken from figure 1:12. Components which become more positive with increasing m cause the oblique instability to be preferred. (*a*) Component U_1, representing the effect of the nonhomogeneous term $-n\bar{w}u_0$ appearing in (2.3) on Ω_2, is destabilizing and effectively independent of m. Component U_2, representing the interaction of the first-order modes is destabilizing, but decreases with increasing m. The only component to increase with increasing m is U_3, representing the effect of the zeroth-order non-homogeneous terms appearing in (2.9) on Ω_2. (*b*) Component U_3 regraphed together with its two parts. Part U_{3a}, representing the effect of the term containing $\bar{w}T_0$ is destabilizing but decreases in magnitude as m increases, inhibiting oblique instability. Part U_{3b}, representing the effect of the term containing $(\mathrm{d}\bar{T}/\mathrm{d}x)u_0$, is stabilizing, but becomes more positive with increasing m sufficiently rapidly to counteract the former effect and cause an oblique instability to be preferred.

where
$$A_j = \frac{\mu_j^2}{2\lambda_j(3n^2+2\mu_j)}, \tag{2.19}$$
$$\lambda_j^2 = \mu_j + a^2, \tag{2.20}$$
and
$$\mu_j^3 + \mu_j + n^2 = 0. \tag{2.21}$$

The values of w_j and B_j are given by (1:B 19) and (1:B 30).

The variables Ω_2 and U_j are plotted versus m in figure 2(*a*) for $\sigma = 5.0$ and $n = 0.38$. As m increases from 0 to 0.5, Ω_2 changes from negative to positive, indicating that a

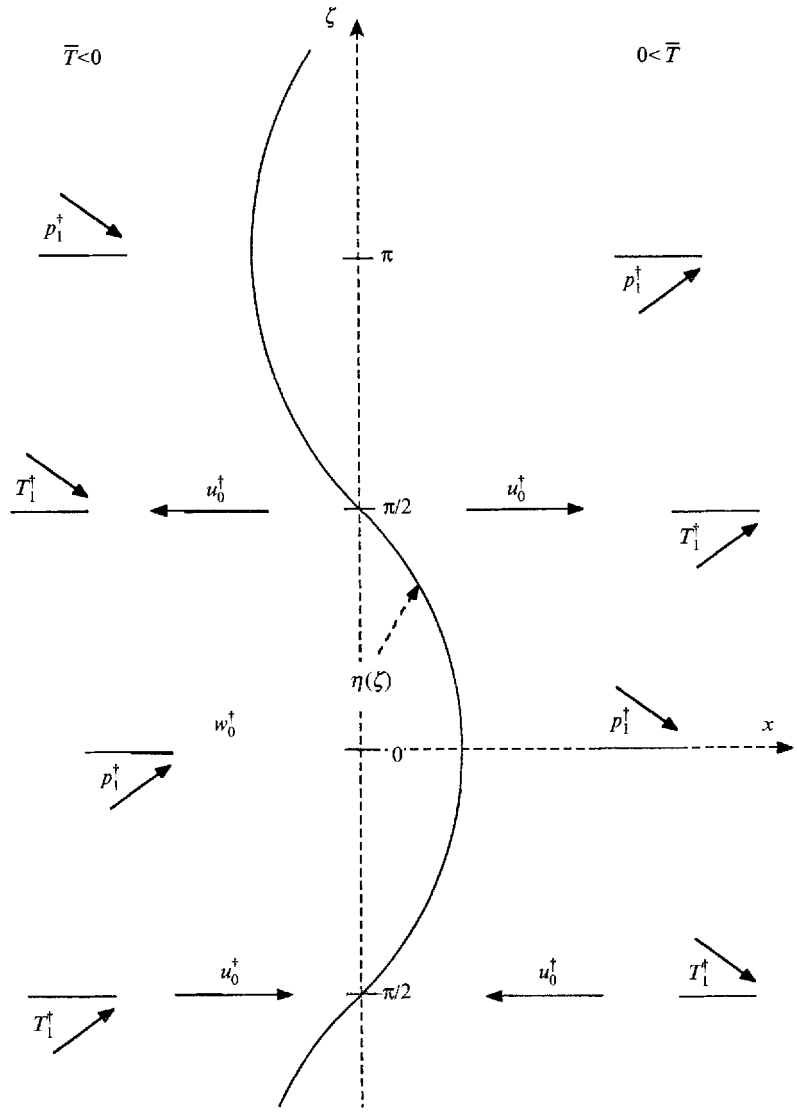

FIGURE 3. A schematic depiction of trends of the variables near the deformed interface with increasing m which leads to an oblique instability. A first-order variable appearing above (below) a horizontal line indicates that it is positive (negative) at that location. A sloping arrow pointing toward the horizontal line indicates that the variable decreases in magnitude with increasing m.

vertical mode is stable for this choice of σ and n, while an oblique mode is unstable. The contribution denoted by U_1 is approximately independent of m and is destabilizing. This represents a mechanical instability akin to the Kelvin–Helmholtz mechanism and is the dominant contribution to Ω_2 for large m. The contribution denoted by U_2 represents the interaction of the first-order modes. Although this contribution is positive and hence destabilizing, it becomes less positive as m increases; that is, it tends to make the vertical mode be preferred. The effect of U_2 is largely counteracted by U_3, representing the effect of the terms proportional to σ appearing in (2.9). This contribution is negative and hence stabilizing but it becomes more positive with increasing m, indicating that this term is the cause of the oblique instability, as previously conjectured.

The individual effect of the two terms contributing to U_3 is quantified in figure 2(*b*). The curve labelled U_{3a} represents the effect of the term containing $\bar{w}T_0$ while that labelled U_{3b} represents the effect of the term containing $(\mathrm{d}\bar{T}/\mathrm{d}x)\,u_0$. Note that these contributions largely cancel, producing a sum U_3 that is significantly smaller than each. The contribution due to $\bar{w}T_0$ is destabilizing but decreases in magnitude as m increases, favouring a vertical instability, while that due to $(\mathrm{d}\bar{T}/\mathrm{d}x)\,u_0$ is stabilizing, but becomes more positive with increasing m sufficiently rapidly to counteract the former effect and cause an oblique instability to be preferred.

The physical mechanism of oblique instability may be summarized using (2.3) and restricting attention to $0 < x$ as follows. The zeroth-order normal velocity, $u_0^\dagger$, is negatively correlated with $\mathrm{d}\tilde{\eta}/\mathrm{d}z$ (see figure 1) but decreases in magnitude with increasing m. This velocity advects the basic-state temperature gradient $(\mathrm{d}\bar{T}/\mathrm{d}x)$ (which is positive for $0 < x$) producing a thermal perturbation, $T_1^\dagger$, which is negatively correlated with $\mathrm{d}\tilde{\eta}/\mathrm{d}z$ and which decreases in magnitude with increasing m. This thermal perturbation produces, via the buoyancy term, a pressure perturbation, $p_1^\dagger$, that is positively correlated with $\tilde{\eta}$ and hence is stabilizing. However, its magnitude decreases with increasing m sufficiently rapidly that an oblique instability is preferred. These interactions are depicted schematically in figure 3.

We anticipate that an oblique mode of instability will be preferred in the present case of a Cartesian plume because in the limit of widely separated interfaces, each behaves as an isolated interface. The precise range of parameters for which oblique instability is preferred is determined by the analyses described in §§4 and 5.

3. Formulation of the problem

We consider an infinite extent of a Boussinesq fluid having a density depending on both temperature, T, and concentration, C, of buoyant material; the Boussinesq equation of state is given by (1:2.1). We assume that in the undisturbed state, the concentration has the 'top-hat' profile (see figure 4):

$$C = \begin{cases} C_0 + \tilde{C} & \text{for} \quad |x| < X_0 \\ C_0 & \text{for} \quad X_0 < |x|, \end{cases} \tag{3.1}$$

forming a Cartesian plume.

The dimensionless governing equations are given by (1:2.7)–(1:2.10). These equations contain two dimensionless parameters: the Prandtl number, σ, and the Reynolds number, R, where

$$\sigma = \nu/\kappa, \quad R = \beta\tilde{C}(g\kappa^3/\alpha^3\gamma^3\nu^5)^{\frac{1}{4}}. \tag{3.2}$$

An additional parameter is the dimensionless plume half-width

$$x_0 = (\alpha\gamma g/\nu\kappa)^{\frac{1}{4}} X_0. \tag{3.3}$$

As in the case of the single interface, the variables may be divided into a *static state*, given by (1:2.12), a steady *basic state*, driven by the forcing and denoted by an overbar, and a *perturbation* of infinitesimal amplitude, ϵ, denoted by a dagger:

$$\left.\begin{aligned} \boldsymbol{u} &= \bar{w}\hat{\boldsymbol{z}} + \epsilon\boldsymbol{u}^\dagger, \quad C = C_0 + \bar{C} + \epsilon C^\dagger, \\ T &= T_0 + (z - z_0)/\sigma R + \bar{T} + \epsilon T^\dagger, \\ p &= p_0 - (z - z_0)/\beta\tilde{C} + (z - z_0)^2/2\sigma R + \bar{p} + \epsilon p^\dagger. \end{aligned}\right\} \tag{3.4}$$

Note that the basic-state velocity has only a vertical component and the basic-state variables are functions only of the normal coordinate, x.

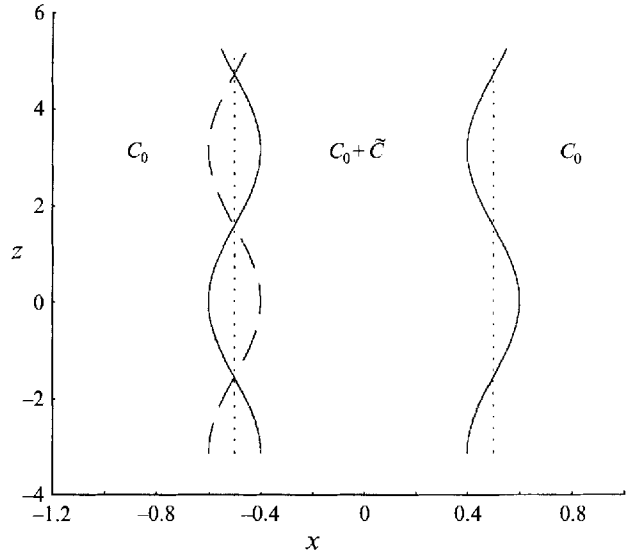

FIGURE 4. A schematic depiction of the Cartesian plume. The dotted line denotes the undeformed position of a plume of width $x_0 = 0.5$. The solid lines denote the positions of the interfaces for a varicose mode as given by (3.7) having $n = 1.0$, $m = 0$ and $\epsilon = 0.1$. The dashed line denotes the position of the left interface for a sinuous mode, given by (3.8). The concentration, C, of buoyant material between the interfaces is larger than that outside.

The basic-state solution, i.e. functions $\bar{w}$ and $\bar{T}$, for the case of two parallel interfaces is given in §3.2 of Part 1. Note that these are even functions of x; expressions valid for $0 < x$ are as follows.

For $0 < x < x_0$:

$$\left.\begin{aligned} \bar{w} &= -\operatorname{Im}[\exp(-kx_0)\cosh(kx)], \\ \bar{T} &= \operatorname{Im}[\mathrm{i}\exp(-kx_0)\cosh(kx)] - 1; \end{aligned}\right\} \tag{3.5}$$

for $x_0 < x$:

$$\left.\begin{aligned} \bar{w} &= \operatorname{Im}[\exp(-kx)\sinh(kx_0)], \\ \bar{T} &= -\operatorname{Im}[\mathrm{i}\exp(-kx)\sinh(kx_0)], \end{aligned}\right\} \tag{3.6}$$

where $k = \sqrt{\mathrm{i}} = (1+\mathrm{i})/\sqrt{2}$.

The perturbation variables are governed by (1:2.16)–(1:2.19). With $\bar{w}$ and $\bar{T}$ being even functions of x, these equations admit solutions of two parities: even parity, having all variables but $\hat{\boldsymbol{x}}\cdot\boldsymbol{u}^\dagger$ even in x, and odd parity, having all variables but $\hat{\boldsymbol{x}}\cdot\boldsymbol{u}^\dagger$ odd in x. We shall see that these parities may be preserved by considering only situations in which the deflections of the two interfaces are out of phase or in phase. If the deflections are out of phase, the plume has a *varicose* shape and the even parity is preserved. If the deflections are in phase, the plume has a *sinuous* shape and the odd parity is preserved. Where necessary in what follows, we shall denote solutions having even parity (varicose mode) by a superscript v, and those having odd parity (sinuous mode) by superscript s; a superscript β will on occasion be used to denote either mode.

The locations of the interfaces of a varicose plume may be described by

$$x^v = \pm[x_0 + \eta(y,z,t)], \tag{3.7}$$

and those of a sinuous plume by

$$x^s = \pm x_0 + \eta(y,z,t) \tag{3.8}$$

(see figure 4) where

$$\eta(y,z,t) = \epsilon\{\exp[\mathrm{i}(my+nz)+\Omega t]+\text{c.c.}\}. \tag{3.9}$$

If $m = 0$ the mode is said to be vertical, while if $m \neq 0$ it is oblique.

As in Part 1 we may assume that the perturbation variables have the same harmonic variation as the interface:

$$\{\boldsymbol{u}^\dagger, p^\dagger, T^\dagger, C^\dagger\} = \{\mathrm{i}u^\beta, v^\beta, w^\beta, \mathrm{i}np^\beta, T^\beta, C^\beta\}\exp[\mathrm{i}(my+nz)+\Omega t)]+\text{c.c.} \tag{3.10}$$

Noting that the perturbation in composition is identically zero (see (1:4.11)), the perturbation equations are (1:4.3), (1:4.5)–(1:4.7) and (1:4.13), which are reproduced here:

$$\mathrm{d}u^\beta/\mathrm{d}x + mv^\beta + nw^\beta = 0, \tag{3.11}$$

$$(\mathrm{d}^2/\mathrm{d}x^2 - a^2 - \bar{\Omega}^\beta)\, v^\beta = -mnp^\beta, \tag{3.12}$$

$$(\mathrm{d}^2/\mathrm{d}x^2 - a^2)\, p^\beta - T^\beta + 2\mathrm{i}Ru^\beta(\mathrm{d}\bar{w}/\mathrm{d}x) = 0, \tag{3.13}$$

$$(\mathrm{d}^2/\mathrm{d}x^2 - a^2 - \bar{\Omega}^\beta)\, w^\beta - \mathrm{i}Ru^\beta(\mathrm{d}\bar{w}/\mathrm{d}x) + T^\beta = -n^2p^\beta, \tag{3.14}$$

$$(\mathrm{d}^2/\mathrm{d}x^2 - a^2 - \sigma\bar{\Omega}^\beta)\, T^\beta - \mathrm{i}\sigma Ru^\beta(\mathrm{d}\bar{T}/\mathrm{d}x) - w^\beta = 0, \tag{3.15}$$

where

$$\bar{\Omega}^\beta = \Omega^\beta + \mathrm{i}nR\bar{w}(x) \tag{3.16}$$

is the Doppler-shifted frequency and a is given by (2.5).

Equations (3.11)–(3.15) are to be solved subject to the conditions that the perturbation variables decay with distance from the interfaces, the full variables (basic state plus perturbation) be continuous across the interfaces and the interfaces be material surfaces. If we take advantage of the parity of the solutions, the conditions on the interface near $x = -x_0$ may be replaced by symmetry conditions at $x = 0$, and attention may then be restricted to $0 < x$. The auxiliary conditions are

$$\text{as } x\to\infty\text{:}\quad u^\beta, v^\beta, w^\beta, p^\beta, T^\beta, \text{ decay to zero;} \tag{3.17a}$$

$$\text{at } x = x_0\text{:}\quad u^\beta, v^\beta, w^\beta, p^\beta, T^\beta, \mathrm{d}v^\beta/\mathrm{d}x \text{ and } \mathrm{d}T^\beta/\mathrm{d}x \text{ are continuous;} \tag{3.17b}$$

$$(\mathrm{d}w^\beta/\mathrm{d}x)_{x=x_0-} = (\mathrm{d}w^\beta/\mathrm{d}x)_{x=x_0+} + 1, \tag{3.17c}$$

$$(\mathrm{d}p^\beta/\mathrm{d}x)_{x=x_0-} = (\mathrm{d}p^\beta/\mathrm{d}x)_{x=x_0+} - 1; \tag{3.17d}$$

$$\text{at } x = x_0\text{:}\quad Ru^\beta = -\mathrm{i}\bar{\Omega}^\beta; \tag{3.17e}$$

at $x = 0$: either

$$u^v = \mathrm{d}v^v/\mathrm{d}x = \mathrm{d}w^v/\mathrm{d}x = \mathrm{d}p^v/\mathrm{d}x = \mathrm{d}T^v/\mathrm{d}x = 0 \quad \text{(even or varicose mode)} \tag{3.17f}$$

or

$$\mathrm{d}u^s/\mathrm{d}x = v^s = w^s = p^s = T^s = 0 \quad \text{(odd or sinuous mode).} \tag{3.17g}$$

Condition (3.17d) may be verified by combining the x-derivative of (3.11) with the normal momentum equation (1:4.4), to obtain

$$\mathrm{d}(mv+nw+np)/\mathrm{d}x + (a^2+\bar{\Omega})\, u = 0. \tag{3.18}$$

Since $\bar{\Omega}$, u and $\mathrm{d}v/\mathrm{d}x$ are continuous across the interface, it follows that $\mathrm{d}(w+p)/\mathrm{d}x$ must be also, and (3.17d) follows from (3.17c). The factor R appears in (3.17e) because the velocity has not been scaled as length divided by time.

As was done in Part 1, the dependent variables and the parameter Ω may be expanded in a power series in R, assuming R to be small:

$$\{u^\beta, v^\beta, w^\beta, p^\beta, T^\beta\} = \sum_{\alpha=0}^{\infty} \{u_\alpha^\beta, v_\alpha^\beta, w_\alpha^\beta, p_\alpha^\beta, T_\alpha^\beta\}\, R^\alpha, \quad \Omega^\beta = \sum_{\alpha=1}^{\infty} \Omega_\alpha^\beta R^\alpha. \tag{3.19}$$

Now

$$\bar{\Omega}^\beta = R[\Omega_1^\beta + \mathrm{i}n\bar{w}(x)] + R^2\Omega_2^\beta + \ldots. \tag{3.20}$$

The principal goal of this paper is determination of the stability of the Cartesian plume. Stability is determined by the first of the sequence $\Omega_1^\beta, \Omega_2^\beta, \ldots$ whose real part is not identically zero for all values of the wavenumbers m and n. We shall see that Ω_1^β is imaginary while Ω_2^β is real, so that it will suffice to solve the sequence Ω_α^β only up to $\alpha = 2$.

Combining (3.17*e*), (3.19) and (3.20) gives

$$\Omega_1^\beta = \mathrm{i}[u_0^\beta(x_0) - n\bar{w}(x_0)], \tag{3.21}$$

and

$$\Omega_2^\beta = \mathrm{i}u_1^\beta(x_0). \tag{3.22}$$

These expressions are to be used to determine the growth rate of the disturbance of the interface.

4. Stability of a thin plume

Before solving the problem of a plume of arbitrary width formulated in §3, it is informative to consider the simpler problem of the instability of a thin plume. The simplified problem is obtained by taking the limit $x_0 \ll 1$. The principal goal of this section is the determination of the functions $\Omega_\alpha^\beta(m, n; x_0, \sigma)$ for $\alpha = 1$ and 2, which describe the stability of the thin Cartesian plume. We shall see that the thin plume is unstable for all values of σ. That is, for every value of σ there exists a set of values of m and n such that either Ω_2^v or Ω_2^s (or both) is positive. Particular attention will be paid to identification of the preferred mode of instability, i.e. the maximum possible value of Ω_2 for given σ and the corresponding values of β, m and n. The principal result of this section is displayed in figure 7.

In the limit $x_0 \ll 1$, the boundary conditions can be reformulated so as to eliminate the region $0 < x < x_0$ from direct consideration. This reformulation takes differing forms for the varicose and sinuous modes. For varicose modes, integration of (3.13)–(3.15) from $x = 0$ to $x = x_0-$ and use of jump conditions (3.17*b–d*), and symmetry conditions (3.17*f*) yields the following:

at $x = x_0+$

$$\left.\begin{gathered} \mathrm{d}w^v/\mathrm{d}x = -1 + O(x_0), \quad \mathrm{d}p^v/\mathrm{d}x = 1 + O(x_0), \\ \mathrm{d}T^v/\mathrm{d}x = 0 + O(x_0), \quad \mathrm{d}v^v/\mathrm{d}x = 0 + O(x_0), \\ u^v + mx_0 v^v + nx_0 w^v + O(x_0^2) = 0. \end{gathered}\right\} \tag{4.1}$$

For sinuous modes, the conditions on v, w, p, and T follow from the Taylor expansions of odd functions plus the jump conditions (3.17*b–d*). The value of u then follows from (3.18).

At $x = x_0+$

$$\left.\begin{gathered} w^s = x_0[\mathrm{d}w^s/\mathrm{d}x + 1] + O(x_0^2), \quad p^s = x_0[\mathrm{d}p^s/\mathrm{d}x - 1] + O(x_0^2), \\ T^s = x_0\,\mathrm{d}T^s/\mathrm{d}x + O(x_0^2), \quad v^s = x_0\,\mathrm{d}v^s/\mathrm{d}x + O(x_0^2), \\ m\mathrm{d}v^s/\mathrm{d}x + n\mathrm{d}(w^s + p^s)/\mathrm{d}x + (a^2 + \bar{\Omega})u^s = 0. \end{gathered}\right\} \tag{4.2}$$

Using (4.1*d*) and (4.2*d*) and noting that $\bar{w}(x_0) \approx x_0/\sqrt{2}$, (3.21) and (3.22) may be expressed as

$$\Omega_1^v = -\mathrm{i}x_0[mv_0^v(x_0) + nw_0^v(x_0) + n/\sqrt{2}], \tag{4.3}$$

$$\Omega_2^v = -\mathrm{i}x_0[mv_1^v(x_0) + nw_1^v(x_0)], \tag{4.4}$$

$$\Omega_1^s = -\frac{\mathrm{i}}{a^2}\left[m\frac{\mathrm{d}v_0^s}{\mathrm{d}x} + n\frac{\mathrm{d}}{\mathrm{d}x}(w_0^s + p_0^s)\right]_{x=x_0} - \mathrm{i}n\frac{x_0}{\sqrt{2}}, \tag{4.5}$$

$$\Omega_2^s = -\frac{\mathrm{i}}{a^2}\left[m\frac{\mathrm{d}v_1^s}{\mathrm{d}x} + n\frac{\mathrm{d}}{\mathrm{d}x}(w_1^s + p_1^s)\right]_{x=x_0} - \frac{\mathrm{i}}{a^2}\left(\Omega_1^s + \frac{\mathrm{i}nx_0}{\sqrt{2}}\right)u_0^s(x_0). \tag{4.6}$$

The variables u_α^β, w_α^β, p_α^β, and T_α^β are found by solving the sequence of problems which result from substitution of assumed forms (3.19) into (3.13)–(3.15) and conditions (4.1)

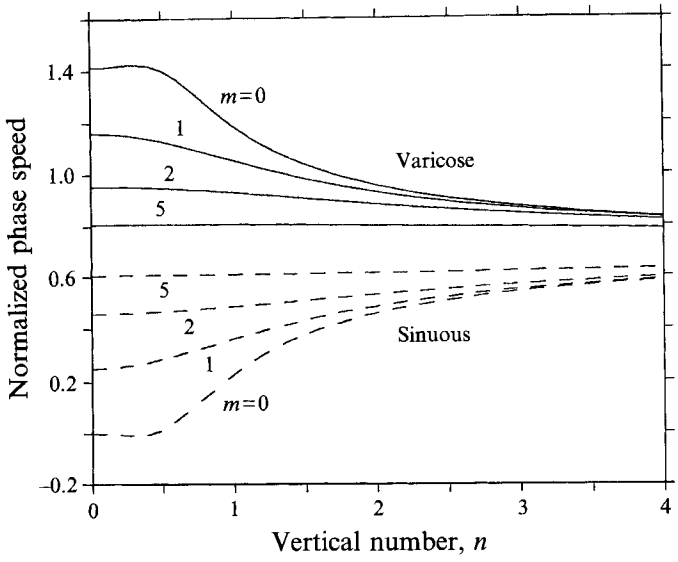

FIGURE 5. A plot of the normalized phase speed, w_{ph}/x_0, of the thin plume versus vertical wavenumber, n, for selected values of the vertical wavenumber m. The solid curves are for the varicose mode and the dashed are for the sinuous mode. A positive phase speed indicates that lines of constant phase move upward. The phase speed of long-wavelength ($n < 0.44$) sinuous modes having very small m is downward relative to the far fluid; all other modes have upward phase speeds. All varicose modes have larger phase speeds than any sinuous mode. As n becomes large all curves approach the asymptote $1/\sqrt{2}$, which represents the normalized speed of the basic state at the edge of the plume. As m becomes large the distinction between varicose and sinuous modes becomes small.

or (4.2); then the functions $\Omega_1^\beta(m, n; x_0, \sigma)$ and $\Omega_2^\beta(m, n; x_0, \sigma)$ are found from (4.3)–(4.6). The details of these calculations are presented in Appendix A which is available from the Journal office or from either author; the results are as follows.

To leading order

$$\Omega_1^\beta(m, n, x_0, \sigma) = -inx_0 \tilde{\Omega}_1^\beta(m, n), \tag{4.7}$$

where

$$\tilde{\Omega}_1^v(m, n) = \frac{1}{\sqrt{2}} - 2\sum_{j=1}^{3} \lambda_j^2 A_j, \tag{4.8}$$

and

$$\tilde{\Omega}_1^s(m, n) = \frac{1}{\sqrt{2}} + 2\sum_{j=1}^{3} \lambda_j^2 A_j, \tag{4.9}$$

where A_j and λ_j are given by (2.19) and (2.20). Note that Ω_1^β is independent of the Prandtl number, σ, and linear in x_0. Also note that

$$\sum_{j=1}^{3} \lambda_j^2 A_j = \tfrac{1}{2} M_3$$

where M_k is defined by (1:4.32).

As in Part 1,

$$\mathrm{Im}\left[\sum_{j=1}^{3} f(\mu_j, \lambda_j, A_j)\right] = 0 \tag{4.10}$$

for any function f. Consequently both Ω_1^v and Ω_1^s are imaginary. As in the case of a single interface, this zeroth-order mode is neutrally stable, but unlike that case, Ω_1 is not zero. The loss of symmetry with the addition of the second interface introduces a phase drift of the neutral distortion. However, as in the case of a single interface, we must go to higher order to determine the stability of the thin plume.

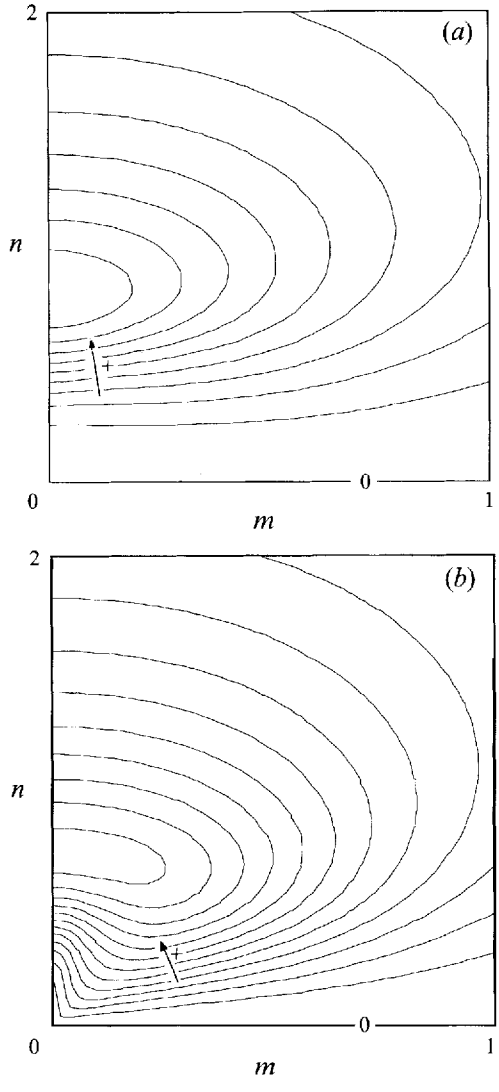

FIGURE 6(*a*,*b*). For caption see facing page.

The phase speed of this neutral disturbance of the plume,

$$w_{ph}^{\beta} = x_0 \tilde{\Omega}_1^{\beta}, \tag{4.11}$$

varies linearly with the plume thickness. The normalized phase speed w_{ph}/x_0 is plotted versus the vertical wavenumber, n, for several values of the horizontal wavenumber, m, in figure 5. Since $M_3 \leqslant 0$ for all values of the wavenumbers, the varicose waves on the interface move upward relative to the local fluid, which has normalized upward speed $1/\sqrt{2}$, while sinuous waves move downward. Relative to the far fluid, all varicose waves move upward, as do all sinuous waves having $0.44 < n$, but those having $0 < n < 0.44$ and m sufficiently small move downward relative to the far fluid. As m and/or n becomes large both types of wave tend to become stationary with respect to the local fluid. Note that the thin-plume analysis is valid provided $nx_0 \ll 1$, so that the vertical wavelength of the disturbance is long compared with the plume thickness. It follows that Ω_1 is small; the waves migrate along the plume slowly.

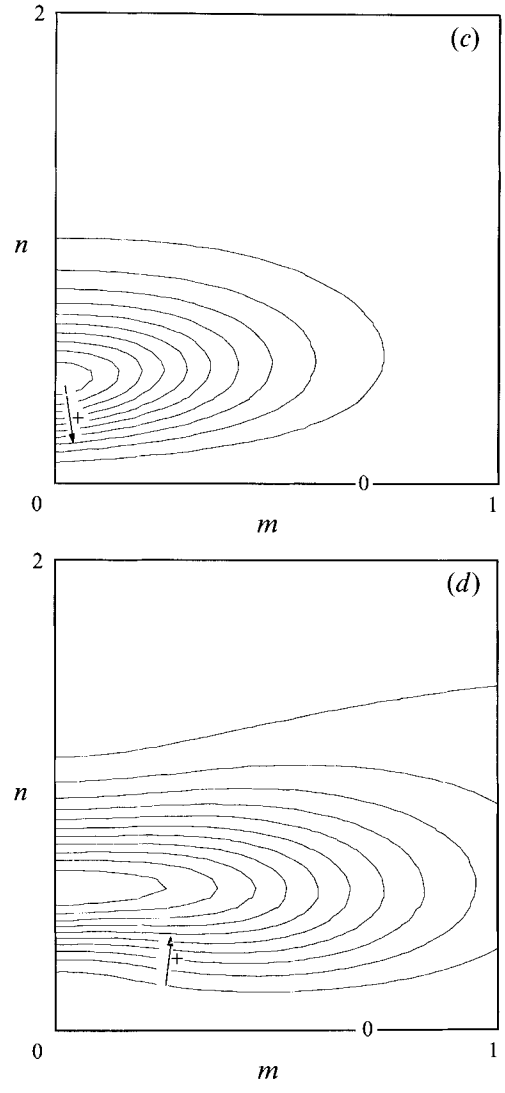

FIGURE 6. Isolines of the normalized growth-rate functions for the thin plume, defined by (4.15), on the (m, n) wavenumber plane. The functions $\tilde{c}_0^s$ and $\tilde{c}_0^v$, whose isolines are plotted in (*a*) and (*b*) respectively, represent the effect of thermal diffusion on the sinuous and varicose modes, and $\tilde{c}_1^s$ and $\tilde{c}_1^v$, whose isolines are plotted in (*c*) and (*d*), represent the effect of viscosity. Contour intervals are 0.01 for (*a*), 0.002 for (*b*), 0.005 for (*c*) and 0.003 for (*d*). Thermal diffusivity destabilizes both modes for all wavenumbers. Viscosity stabilizes the varicose mode for all wavenumbers and destabilizes the sinuous mode for moderate and small values of the vertical wavenumber, n; viscosity weakly stabilizes the sinuous mode for large values of n.

To next order in powers of R, Ω_2 is real, and the stability of the plume is determined. The expressions for $\Omega_2^\beta(m, n; x_0, \sigma)$ are developed in Appendix A on file in the Journal office. Each of these varies as x_0^2; a vanishingly thin plume is neutrally stable. Also, as in the case of a single plane interface, each is a linear function of the Prandtl number, σ, with the portions independent of σ representing the effect of thermal diffusivity while those proportional to σ represent viscosity.

We may write

$$\Omega_2^\beta(m, n; x_0, \sigma) = x_0^2 \tilde{\Omega}_2^\beta(m, n; \sigma), \tag{4.12}$$

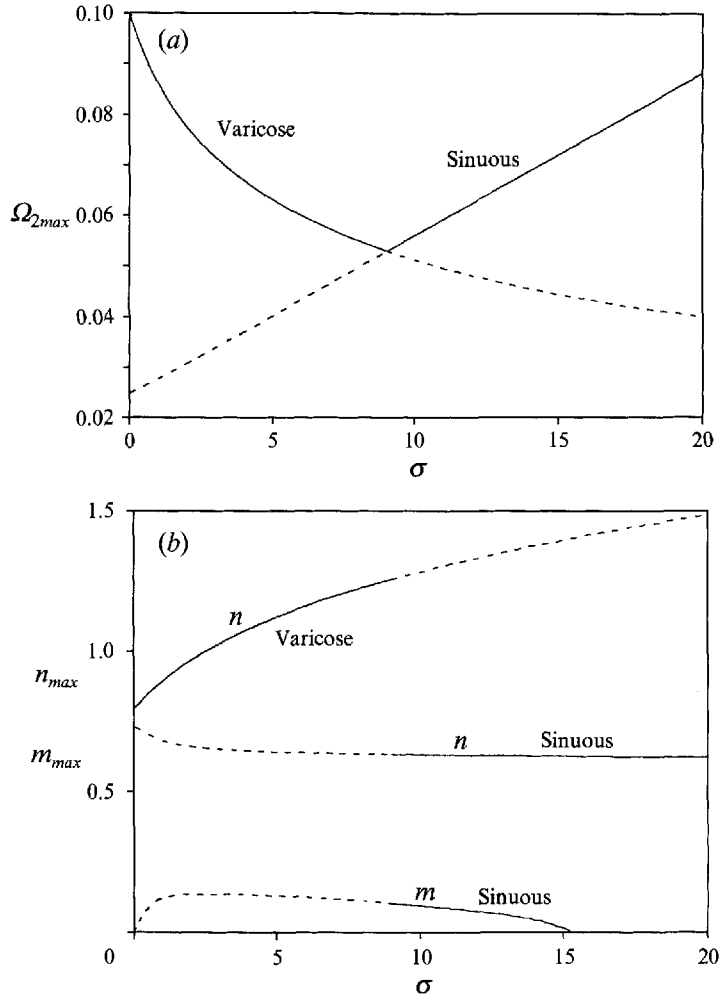

FIGURE 7. Plots of the maximum normalized growth rate $\tilde{\Omega}_{2max}$ (in a) and the optimal wavenumbers (in b) versus the Prandtl number σ for the sinuous and varicose modes for the thin plume. The preferred mode is indicated by the solid lines. The varicose mode is preferred if $\sigma < 9.06$, while the sinuous mode is preferred for larger Prandtl numbers. The maximum growth rate decreases with increasing σ for $\sigma < 9.06$, and grows roughly linearly for $9.06 < \sigma$. The preferred varicose mode is vertical ($m = 0$) while the preferred sinuous mode is oblique for $9.06 < \sigma < \sim 15$ and vertical for larger values of σ.

where the normalized growth rate $\tilde{\Omega}_2^\beta$ is known to be linear in σ:

$$\tilde{\Omega}_2^\beta(m,n;\sigma) = \tilde{c}_0^\beta(m,n) + \sigma\tilde{c}_1^\beta(m,n). \tag{4.13}$$

This functional dependence is virtually identical to that for the single plane interface; compare (4.13) with (1:4.30). The only difference is that there are two modes to consider in the present case, while only one exists for the single interface. As in that case, the stability character may be deduced from the isoline plots of the functions $\tilde{c}_j^\beta(m,n)$. These plots are presented in figure 6, with parts $(a),(b),(c),(d)$ showing $\tilde{c}_0^v, \tilde{c}_0^s$, $\tilde{c}_1^v, \tilde{c}_1^s$, respectively. These plots should be compared with those in figure 1:11.

Recalling that the term $\tilde{c}_0^\beta$ may be thought of as representing the effect of thermal diffusivity while $\tilde{c}_1^\beta$ represents viscosity, it may be deduced from these plots that thermal diffusion is destabilizing for both varicose and sinuous modes, while viscous diffusion

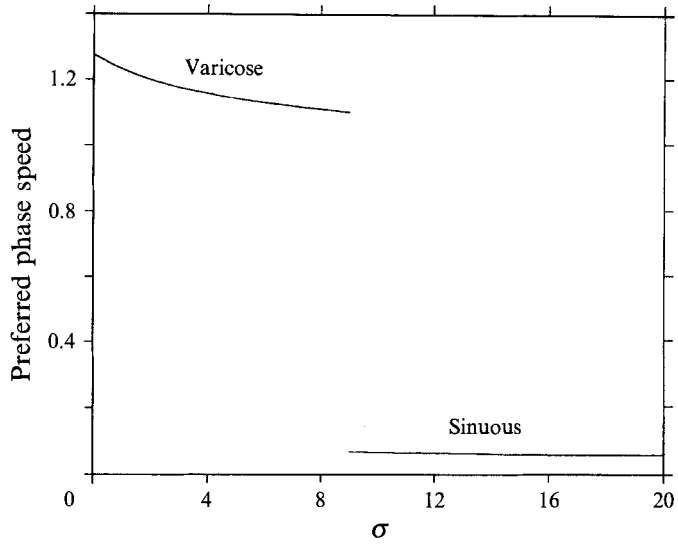

FIGURE 8. A plot of the phase speed of the preferred mode versus the Prandtl number σ for the thin plume.

stabilizes the varicose mode, but destabilizes the sinuous mode. The destabilizing effect of thermal diffusivity may be understood by the discussion presented in §2 and the stabilization of the varicose mode by viscosity is as expected, but the destabilization of the sinuous mode by viscosity is unexpected.

For small Prandtl number, the varicose mode is more unstable than the sinuous mode. As the Prandtl number increases from zero, the varicose mode becomes less unstable, with the preferred mode shifting to larger values of n. At the same time, the sinuous mode becomes more unstable, with a slight shift of the preferred mode to smaller values of n.

The preferred mode of instability and the associated maximum growth rate may be found by maximizing expression (4.13) for $\tilde{\Omega}_2^\beta$ over all m and n for both parities for a specified value of σ. The results are presented in figure 7, which contains in part (*a*) a plot of $\tilde{\Omega}_{2max}$ and in part (*b*) m_{max} and n_{max} versus σ. This plot should be compared with figure 1:12. From this it may be seen that the varicose mode is preferred for Prandtl numbers smaller than ~ 9 while the sinuous mode is preferred for larger Prandtl numbers. The preferred varicose mode always is vertical (i.e. has a horizontal wavenumber, m, of zero), while the preferred sinuous mode is oblique for Prandtl numbers less than ~ 15. Thus the preferred mode has a non-zero horizontal wavenumber for $\sim 9 < \sigma < \sim 15$. The preferred wavenumber jumps discontinuously at the cross-over value ~ 9, while the preferred growth rate varies continuously. The effect of a non-zero horizontal wavenumber on the preferred mode is small. If we set $m = 0$, the cross-over point becomes $\sigma = 9.255$, and the value of $\tilde{\Omega}_{2max}$ is changed only slightly. The preferred modes of the thin plume may be summarized as follows:

$0 < \sigma < \sim 9$ varicose vertical;

$\sim 9 < \sigma < \sim 15$ sinuous oblique;

$\sim 15 < \sigma$ sinuous vertical.

Combining figures 5 and 7, yields the preferred phase speed given in figure 8. The phase speed decreases smoothly from 1.28 at $\sigma = 0$ to 1.10 for $\sigma \sim 9$, then decreases sharply to 0.07 and decreases very slowly with increasing σ thereafter.

5. Stability of a plume of arbitrary width

We now consider general stability problem formulated in §3. As in §4, the goal of the analysis is evaluation of the functions $\Omega_1^\beta(m,n;x_0,\sigma)$ and $\Omega_2^\beta(m,n;x_0,\sigma)$, from which the stability of the plume may be determined. We shall see that the plume is unstable for all prescribed values of x_0 and σ. That is, for every set of values of (x_0,σ) there exists a set of values of m and n such that either Ω_2^v or Ω_2^s (or both) is positive. In this section, particular attention will be paid to identification of the preferred mode of instability, i.e. the maximum possible value of Ω_2 for given x_0 and σ and the corresponding values of β, m and n. The preferred modes may be characterized as either varicose or sinuous and either vertical ($m=0$) or oblique, giving a total of four types of modes. The principal result of this section is the regime diagram given in figure 11, showing the preferred modes on the (x_0,σ)-plane.

The necessary calculations are outlined in Appendix B available from the Journal office or from either author, and the results are summarized in the following. It should be noted that these results are subject to two stringent checks: as x_0 becomes large, the results should agree with those of Part 1, while as $x_0\to 0$, the results should agree with those of §4. Appendix C containing a calculation showing that as $x_0\to 0$ the results obtained in Appendix B agree with those in Appendix A is available from the Journal office or from either author.

To dominant order in R, Ω is independent of σ:

$$\Omega_1^\beta(m,n;x_0,\sigma) = -\mathrm{i}n\hat{\Omega}_1^\beta(m,n;x_0), \tag{5.1}$$

for $\beta = v,s$ where

$$\hat{\Omega}_1^v = \tfrac{1}{2}\sin(\sqrt{2}x_0)\exp(-\sqrt{2}x_0) + \sum_{j=1}^{3}\lambda_j A_j \exp(-2\lambda_j x_0), \tag{5.2}$$

and

$$\hat{\Omega}_1^s = \tfrac{1}{2}\sin(\sqrt{2}x_0)\exp(-\sqrt{2}x_0) - \sum_{j=1}^{3}\lambda_j A_j \exp(-2\lambda_j x_0). \tag{5.3}$$

The expressions Ω_1^β are imaginary, indicating neutral stability to this order. As x_0 becomes small, these expressions reduce to those given by (4.7)–(4.9). In the limit $x_0\to\infty$, $\Omega_1^\beta\to 0$, in agreement with (1:4.22).

As in the cases of a single plane interface and a thin Cartesian plume, Ω_2^β is real and linear in the Prandtl number, σ:

$$\Omega_2^\beta(m,n;x_0,\sigma) = c_0^\beta(m,n,x_0) + \sigma c_1^\beta(m,n,x_0). \tag{5.4}$$

The extreme (maximum and minimum) values of c_0^β and c_1^β over all possible values of m and n are plotted versus x_0 in figure 9, with the maximum values of c_0 given in part (*a*), the maximum values of c_1 in part (*b*) and the minimum values of c_1 in part (*c*). The minimum values of c_0 (not shown) are identically zero.

It may be seen from figure 9 that the difference between the varicose and sinuous values becomes small as x_0 becomes large, as anticipated. The value of c_0 is always positive, indicating that thermal diffusivity is always destabilizing. Also, c_1 may have positive values, particularly for moderate values of x_0, indicating that viscosity may be destabilizing. The maximum values of c_0 and c_1 occur for values of x_0 between 1 and 3, suggesting that plumes of these widths are more unstable than those which are either thinner or thicker. For moderate values of x_0, the sinuous mode is preferred when σ is small, while the varicose mode is preferred for large σ.

The wavenumbers associated with the maximum and minimum values of c_0 and c_1

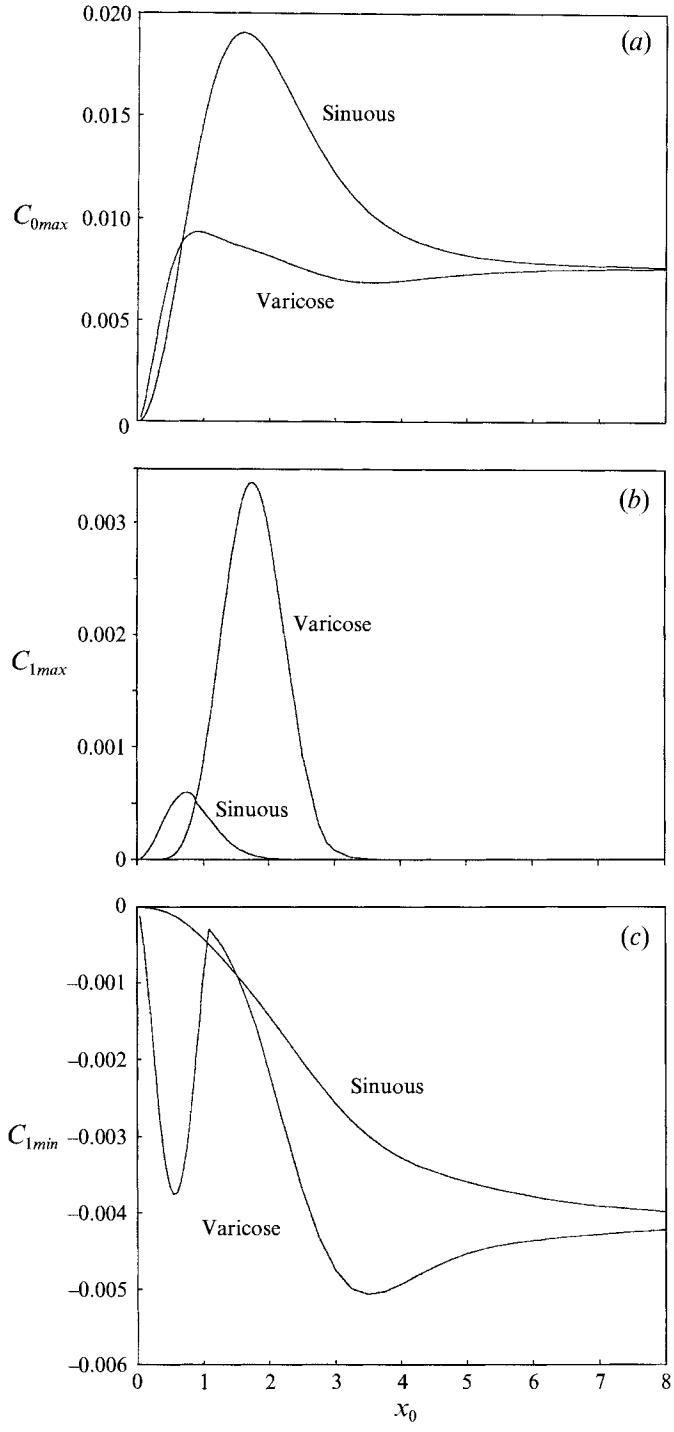

FIGURE 9. Plots versus x_0 of the maximum values of c_0 (in *a*) and c_1 (in *b*), and the minimum value of c_1 (in *c*). (The minimum of c_0 is exactly zero.)

are displayed in figure 10, with m and n for c_0 maximum given in part (a), m and n for c_1 maximum given in part (b) and n for c_1 minimum given in part (c). The optimal values of m for c_1 minimum are identically zero. It may be seen that the maximum values typically occur for oblique modes (having $m \neq 0$). A mode shift occurs near $x_0 = 1.08$ in the preferred varicose minimum of c_1.

The results shown in figures 9 and 10 (plus some additional data for larger values of x_0) may be used to determine the nature of the preferred modes for the two limits $\sigma = 0$ and $\sigma = \infty$. For $\sigma = 0$, the preferred modes as a function of x_0 are

$$\begin{aligned} &0 < x_0 < 0.67 && \text{varicose vertical;} \\ &0.67 < x_0 < \sim 4.9 && \text{sinuous vertical;} \\ &\sim 4.9 < x_0 < \sim 8.6 && \text{sinuous oblique;} \\ &\sim 8.6 < x_0 && \text{sinuous vertical.} \end{aligned}$$

For $\sigma = \infty$, the preferred modes as a function of x_0 are

$$\begin{aligned} &0 < x_0 < 0.88 && \text{sinuous vertical;} \\ &0.88 < x_0 < 3.56 && \text{varicose oblique;} \\ &3.56 < x_0 < \sim 5.0 && \text{sinuous oblique;} \\ &\sim 5.0 < x_0 && \text{varicose oblique.} \end{aligned}$$

The preferred mode in general is that which has the most rapid growth rate for given values of x_0 and σ, and is obtained by maximizing Ω_2^β over m and n for both $\beta = v$ and $\beta = s$. The result of this operation is summarized in a regime diagram given in figure 11. This displays the (x_0, σ)-plane, divided into four regimes labelled Sv, So, Vv and Vo, corresponding to the four possible types of modes previously identified, i.e. sinuous vertical, sinuous oblique, varicose vertical and varicose oblique. Note that this diagram is consistent with (i) the results given in Part 1 as $x_0 \to \infty$, (ii) with the results given in §4 as $x_0 \to 0$ and (iii) with the summary given in the previous paragraph in the limits $\sigma \to 0$ and $\sigma \to \infty$; specifically, the isoline plots given in figures 1:11 and 6 correspond to and agree with the corners of figure 11, while the curves of maximum growth rate and preferred wavenumber given in figures 1:12, 7, 9 and 10 correspond to and agree with the edges of figure 11. Figure 11 shows no clear pattern of preferred mode, with each of the four types of modes being preferred in at least one region. The sinuous oblique mode is preferred for large values of x_0, but the distinction between sinuous and varicose modes fades as x_0 becomes large (e.g. see figures 9 and 10). The growth rate is largest in region Vo; see figure 9(b) for the growth rate when $\sigma = \infty$.

6. Summary

The stability of two plane parallel vertically oriented interfaces within an infinite extent of fluid has been investigated, in the case that there are identical sharp jumps in composition across each interface, such that the fluid between the interfaces has one composition and that outside the interfaces has another. Material diffusivity is neglected, so that the interfaces remain sharp and identifiable. A density jump is assumed to accompany the jump in composition, and this acts to drive vertical motions parallel to the unperturbed interfaces. The entire fluid has a stabilizing vertical temperature gradient, so that the basic-state vertical motion tends to induce a local change in temperature which is balanced by lateral thermal diffusion. We investigate the stability of this basic state and of the shapes of the two interfaces.

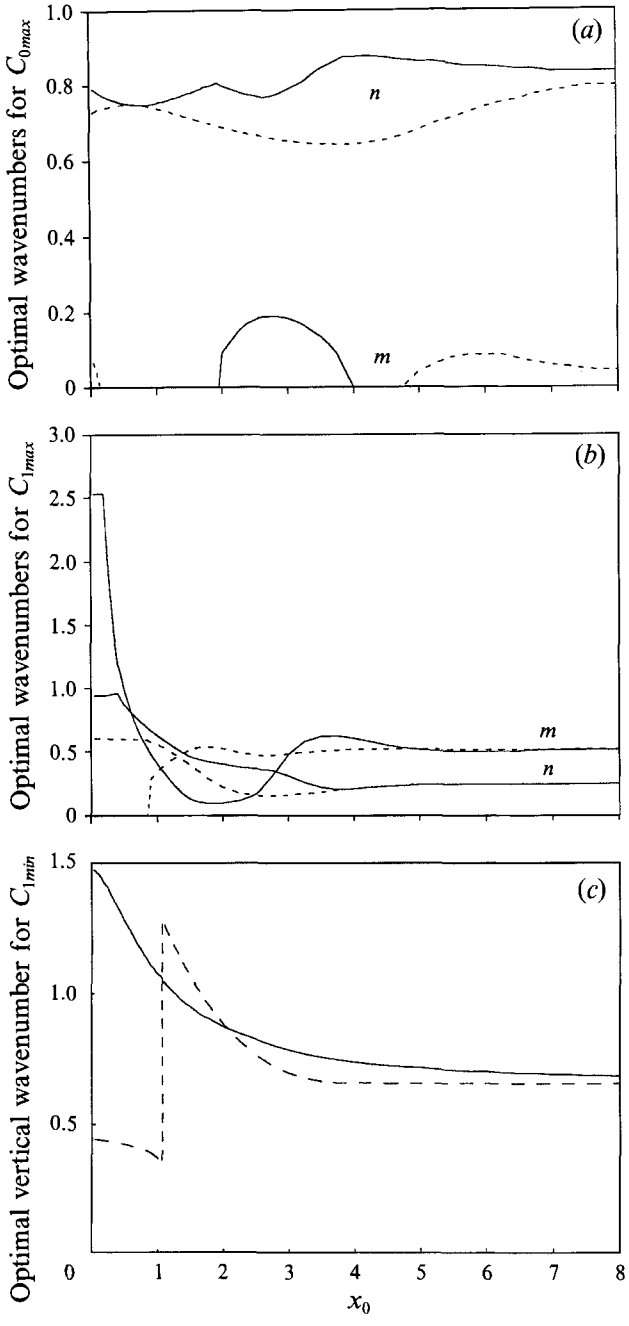

FIGURE 10. Pots versus x_0 of the optimal values of wavenumbers m and n which achieve the maxima plotted in figure 9: (*a*), (*b*), and (*c*) correspond to (*a*), (*b*), and (*c*) of figure 9. In each part, the solid curve indicates the sinuous mode and the dashed curve indicates the varicose mode. Note that all minima of c_1 occur for $m = 0$.

The governing equations admit solutions with even or odd parities. These parities are best remembered by the corresponding shapes of the deformed interfaces: either varicose (even parity) or sinuous (odd parity). The case of closely spaced interfaces (i.e. a thin plume) is treated separately (in §4) from the general case of interfaces having

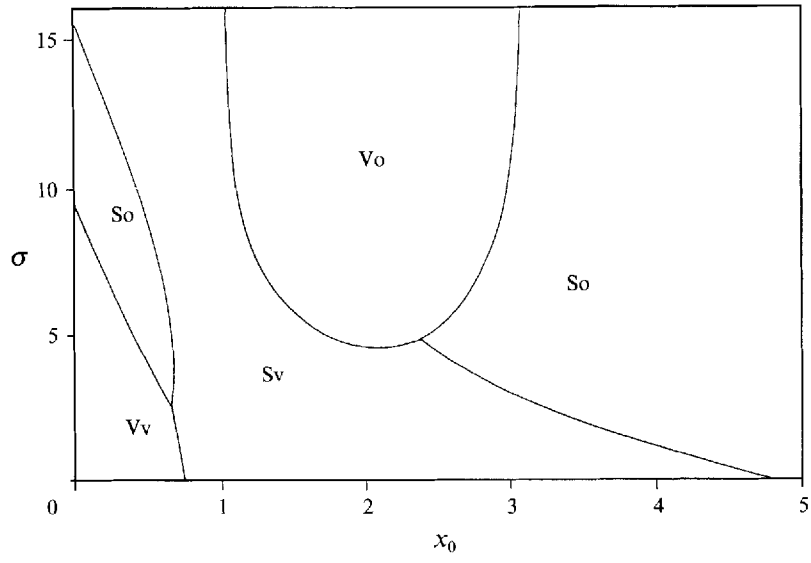

FIGURE 11. Regime diagram, displaying on the (x_0, σ)-plane locations where the preferred mode is either sinuous vertical (Sv), sinuous oblique (So), varicose vertical (Vv) or varicose oblique (Vo). The distinction between varicose and sinuous modes fades as x_0 increases; differences in the growth rates are less than 1% for x_0 greater than about 7. Isoline plots of the growth rates of the varicose and sinuous modes on the (m,n)-plane corresponding to the corners of this figure are given as follows: (i) for $x_0 = 0$ and $\sigma = 0$ in figures 6(*a*) and 6(*b*), (ii) for $x_0 = 0$ and $\sigma = \infty$ in figures 6(*c*) and 6(*d*), (iii) for $x_0 = \infty$ and $\sigma = 0$ in figure 1:11(*a*) and (iv) for $x_0 = \infty$ and $\sigma = \infty$ in figure 1:11(*b*). Curves of the maximum value of Ω_2 and the optimal values of m and n for the four edges of this figure are given as follows: (i) $x_0 = 0$ in figures 7(*a*) and 7(*b*), (ii) $\sigma = 0$ in figures 9(*a*) and 10(*a*), (iii) $x_0 = \infty$ in figure 1:12 and (iv) $\sigma = \infty$ in figures 9(*b*) and 10(*b*).

arbitrary spacing (in §5). The results of the general case are found to agree both with those of the single interface found in Part 1 and with those of the thin plume, providing a strong check on the accuracy of all three results.

It is found that the flows and interface shapes are unstable for some wavenumber for all values of the Prandtl number and interface spacing. Four possible modes of instability are identified, i.e. sinuous vertical, sinuous oblique, varicose vertical and varicose oblique. The principal results of the stability analyses for the thin plume and general plume are presented in figures 7 and 11. Figure 7(*a*) shows for the thin plume that the varicose mode is most unstable for Prandtl number $\sigma < \sim 9$ while the sinuous mode is preferred for larger value of σ, while it may be seen from figure 7(*b*) that the preferred varicose mode is vertical, while the sinuous mode is oblique for $\sim 9 < \sigma < \sim 15$ and vertical for larger values. Figure 11 displays the regime diagram for the general plume on the (x_0, σ)-plane. This plane is divided into regimes labelled Sv, So, Vv and Vo, corresponding to which of the four possible modes is dominant for that value of x_0 and σ. There is no clear pattern of preference, except that the sinuous oblique mode is preferred for a wide plume. The growth rate is largest for plumes of dimensionless width between 1 and 3.

This work was supported in part by grants EAR-8520678, EAR-8805349 and EAR-9116959 from the Earth Sciences Section of the National Science Foundation. This is publication #355 of the Geophysical Fluid Dynamics Institute, Florida State University, Tallahassee, Florida.

REFERENCES

DRAZIN, P. G. & REID, W. H. 1981 *Hydrodynamic Stability*. Cambridge University Press.

DUDIS, J. J. & DAVIS, S. H. 1971 Energy stability of the buoyancy boundary layer. *J. Fluid Mech.* **47**, 381–403.

ELTAYEB, I. A. & LOPER, D. E. 1991 On the stability of vertically oriented double-diffusive interfaces. Part 1. A single plane interface. *J. Fluid Mech.* **228**, 149–181.

GILL, A. E. 1966 The boundary-layer regime for convection in a rectangular cavity. *J. Fluid Mech.* **26**, 515–536.

GILL, A. E. & DAVEY, A. 1969 Instabilities of a buoyancy-driven system. *J. Fluid Mech.* **35**, 775–798.

HINCH, E. 1984 A note on the mechanism of the instability at the interface between two shearing fluids. *J. Fluid Mech.* **144**, 463–465.

HOLYER, J. Y. 1983 Double-diffusive interleaving due to horizontal gradients. *J. Fluid Mech.* **137**, 347–362.

LISTER, J. R. 1987 Long-wavelength instability of a line plume. *J. Fluid Mech.* **175**, 413–428.

SCHNEIDER, W. 1981 Flow induced by jets and plumes. *J. Fluid Mech.* **108**, 55–65.